Nanotubular J-Aggregates and Quantum Dots Coupled for Efficient Resonance Excitation Energy Transfer

Yan Qiao,*[,†,∥,§] Frank Polzer,[†,⊥] Holm Kirmse,[†] Egon Steeg,[†] Sergei Kühn,[‡] Sebastian Friede,[‡] Stefan Kirstein,*[,†] and Jürgen P. Rabe[†,∥]

[†]Department of Physics, Humboldt-Universität zu Berlin, Newtonstr 15, 12489 Berlin, Germany, [∥]IRIS Adlershof, Humboldt-Universität zu Berlin, Zum Großen Windkanal 6, 12489 Berlin, Germany, and [‡]Nichtlineare Optik und Kurzzeitspektroskopie im Forschungsverbund Berlin e.V., Max-Born-Institut, Max-Born-Straße 2 A, 12489 Berlin, Germany. [§]Present address: Centre for Protolife Research and Centre for Organized Matter Chemistry, School of Chemistry, University of Bristol, Bristol BS8 1TS, United Kingdom. [⊥]Present address: Materials Science & Engineering, University of Delaware, Newark, DE 19716, USA.

ABSTRACT Resonant coupling between distinct excitons in organic supramolecular assemblies and inorganic semiconductors is supposed to offer an approach to optoelectronic devices. Here, we report on colloidal nanohybrids consisting of self-assembled tubular J-aggregates decorated with semiconductor quantum dots (QDs) *via* electrostatic self-assembly. The role of QDs in the energy transfer process can be switched from a donor to an acceptor by tuning its size and thereby the excitonic transition energy while keeping the chemistry unaltered. QDs are located within a close distance (<4 nm) to the J-aggregate surface, without harming the tubular structures and optical properties of J-aggregates. The close proximity of J-aggregates and QDs allows the strong excitation energy transfer coupling, which is around 92% in the case of energy transfer from the QD donor to the J-aggregate acceptor and approximately 20% in the reverse case. This system provides a model of an organic–inorganic light-harvesting complex using methods of self-assembly in aqueous solution, and it highlights a route toward hierarchical synthesis of structurally well-defined supramolecular objects with advanced functionality.

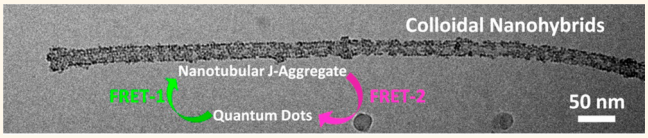

KEYWORDS: Förster resonance energy transfer (FRET) · organic–inorganic hybrid system · amphiphilic cyanine dye · semiconductor · CdTe · self-assembly · light harvesting

Nanoscale integration of organic and inorganic materials is currently a hot research topic because the combination of both materials is anticipated to open up new avenues for the design of high-performance devices. The prospect results from the synergistic advantage when both material types contribute with their specific features, such as high oscillator strength of the organic phase and high stability of the inorganic phase. One of the main challenges lies in the precise structural organization of such materials on the nanometer scale, since the functionality crucially depends on the correct composition and mutual alignment of the molecular assemblies and the inorganic nanostructures. Therefore, there is a high demand for a reliable strategy to build hybrid systems with controllable structure and morphology

A strong electronic coupling between organic and inorganic types would bring new features that cannot be obtained from a single component. One prominent example of the attractive functionality of hybrid nanosystems is resonant dipole–dipole coupling between an organic assembly and inorganic semiconductors.[1−4] The coupling within such a hybrid system takes place between two distinct excitons. Particularly promising for outstanding nonlinear properties are extended Frenkel exciton systems,[5] such as in J-aggregates, formed by organic assemblies of amphiphilic cyanine dyes.[6−9] Typically, the excitons within J-aggregates are delocalized over more than 10 molecules,[10,11] leading to large oscillator strengths, big spectral red shifts, and intense but narrow absorption and emission bands. On the other hand, key ingredients are inorganic species such as semiconductor or quantum dots (QDs), exhibiting superior photostability, high fluorescence quantum yield, and size-tunable optical properties.[12,13] The optimization of

* Address correspondence to yanqiao@pku.edu.cn, kirstein@physik.hu-berlin.de.

Received for review October 25, 2014 and accepted January 2, 2015.

Published online January 02, 2015
10.1021/nn506095g

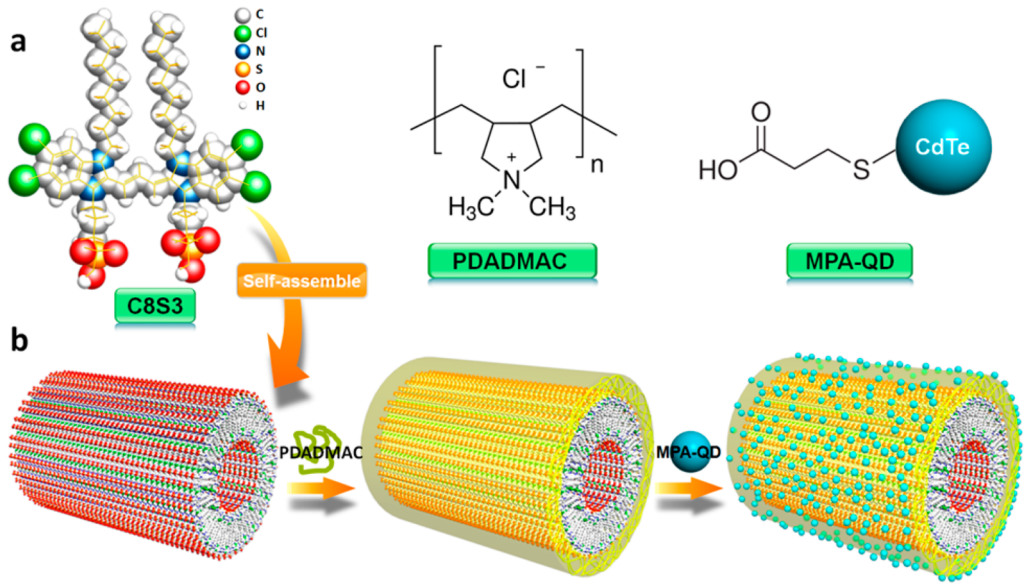

Figure 1. Colloidal J-aggregate/QD nanohybrid formed by an electrostatic self-assembly method in solution. (a) Chemical structures of the constituents: amphiphilic cyanine dye C8S3, PDADMAC, and MPA-capped CdTe QDs; (b) sketch of electrostatic self-assembly toward J-aggregate/QD nanohybrids, in which PDADMAC polycation acts as molecular glue.

such heterostructures ultimately depends upon the precise nanoscale positioning of the individual materials, which is a challenging objective.[14−20] Recently, resonance excitation energy transfer, also named Förster resonance energy transfer (FRET), in J-aggregate/QD systems has been developed on solid substrates using films of blends of the materials[21] or *via* layer-by-layer (LBL) technique.[22] Another application was color-selective photocurrent enhancements observed in coupled J-aggregate/CdSe nanowires.[23] However, to meet the demands of further applications, methods are required to create novel hybrid nanostructures as complete functional entities with nanometer dimensions.

Here we present a new approach to fabricate quasi-one-dimensional (1D) colloidal systems in aqueous solution. Tubular J-aggregates from self-assembled amphiphilic dyes, as investigated and described in detail elsewhere,[24−27] serve as a scaffold for hybrid assembly. In these systems, dye molecules are precisely arranged into closely packed and long-range-ordered structures. Therefore, these aggregates are considered as model systems to mimic complex supramolecular assemblies in biology, such as the light-harvesting center (LHC) of plant and green sulfur bacteria.[28] Such synthetic analogues could ultimately pave the way for fast excitation energy transfer over hundreds of molecules, enabling the mimicking of energy migration and charge transfer processes as observed in natural LHCs. Herein the tubular J-aggregates are used as building blocks for studies of the resonant dipole−dipole coupling with inorganic semiconductor nanoparticles. To this end, we developed a self-assembly strategy to electrostatically combine the semiconductor QDs and J-aggregates by utilizing a polycation as "molecular glue". The J-aggregate/QD hybrids are highlighted not only by the robust and high efficient excitonic transitions at room temperature but also by their thread-like structure providing quasi-1D colloidal behavior.[29] The structural features can offer a large surface area with multiple functionalization sites and high colloidal stability which facilitates practical applications.

RESULTS AND DISCUSSION

Fabrication and Structure of QD-Decorated Tubular J-Aggregates. The chemical structure of the amphiphilic cyanine dye 3,3′-bis(2-sulfopropyl)-5,5′,6,6′-tetrachloro-1,1′-dioctylbenzimidacarbocyanine (C8S3), poly(diallyldimethylammonium chloride) (PDADMAC), and 3-mercaptopropionic acid (MPA)-capped CdTe QDs are shown in Figure 1a. When dissolved in a water/methanol mixture (100:13 by volume), the dye C8S3 self-assembles into double-walled tubular J-aggregates with an outer diameter of 13 ± 1 nm, an inner diameter of 6 ± 1 nm, and lengths up to several tens of micrometers.[18−20] The tubular aggregates exhibit the typical spectroscopic features of J-aggregates, namely, a large red shift in the absorption spectrum compared to the monomer absorption, due to strong excitonic coupling (Supporting Information, Figure S1).[20] Using the supramolecular nanotubes as supporting scaffolds, an electrostatic self-assembly strategy is proposed to fabricate structurally well-defined colloidal nanohybrid systems (Figure 1b). Since a C8S3 molecule possesses two hydrophilic sulfonic groups oriented toward the nanotube's wall surface, the surfaces of the tubular J-aggregates are negatively charged. This negative surface potential leads to an electrostatically driven adsorption of the cationic polyelectrolyte PDADMAC, which covers the outer surface of the nanotubes and thereby reverses

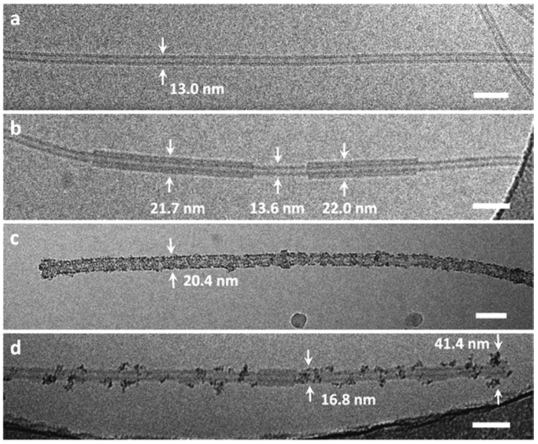

Figure 2. Representative cryo-TEM images of (a) plain tubular J-aggregate showing the typical diameter of 13.0 nm; (b) nanotubular J-aggregate coated by PDADMAC layer, and partially a second dye bilayer; and (c,d) J-aggregate/QD-535 nanohybrids formed by an electrostatic self-assembly method. (c,d) Images taken from the same sample showing the coexistence of different structural motifs (scale bar = 50 nm).

the surface potential (from negative to positive). Subsequently added MPA-capped QDs (negatively charged) bind onto the polycation chains on the outer surface of the tubular aggregates. Thereby, the PDADMAC layer serves as molecular glue that binds the J-aggregate and the QDs together. CdTe QDs of different sizes were employed in order to obtain nanohybrid systems with different energy transfer pathways: the energy transfer from the semiconductors to the J-aggregates was achieved by using QDs with emission centered at 535 nm (QD-535) as donors, while energy transfer from J-aggregates to semiconductors was obtained by using QDs with emission centered at 655 nm (QD-655) as acceptors.

Cryo-transmission electron microscopy (cryo-TEM) was employed to directly visualize J-aggregate/QD nanohybrids as demonstrated in Figure 2. A plain tubular J-aggregate without polycation coverage is represented in Figure 2a, showing the typical outer diameter of 13.0 nm. After the addition of PDADMAC, the tubular morphology of the C8S3 J-aggregate remains intact and its diameter stays almost unchanged, except for an increase of roughly 0.6 nm within the error of the measurement. This is attributed to the coverage of a thin positively charged PDADMAC layer, which is not directly visible by cryo-TEM. Interestingly, parts of the nanotubular J-aggregates exhibit walls, which are thickened by approx. 3.8−4 nm (Figure 2b). The wall thickness within these segments is a bit more than twice as thick as the original J-aggregates, indicating that those fragments contain of a second bilayer of the dye. The coverage of the J-aggregates by PDADMAC was proven by surface charge reversal of the nanotubes.[14] Further evidence is the adsorption of the negatively charged CdTe QDs, as shown in Figure 2c. No adsorption of QDs could be observed when using plain J-aggregates that exhibit a negative surface potential. As can be seen in Figure 2c, the structural feature of the J-aggregates is mostly preserved after addition of CdTe QD-535, and the QDs are only found at the surface of the nanotubes. These nanohybrids can be micrometers long, similar to the bare J-aggregates (Supporting Information, Figure S2). Interestingly, the QDs preferentially bind onto the thin part of the tubes and do not adsorb at the thickened fragments (Figure 2d), which supports the assignment of the thick fragments to a second bilayer of dye, if only the thin part of the aggregate is covered by polycations. In Figure 2d, some QDs are found to be less strictly bound to the surface of the J-aggregates, giving the nanotube a thorn-like appearance. Nevertheless, the majority of QDs are located within a cylinder with a total diameter of 20.4 ± 0.5 nm (as depicted in Figure 2c). This means that the distance between the center of the QDs and the dye molecules, denoted as center-to-center distance r, must be less than 4 nm. For QDs located at the "thorns", the mean distance exceeds 15 nm. However, from inspection of many cryo-TEM images, we can state that the particles within these thorn-like extrusions are the minority.

The adsorption of QD-665 leads to similar structures (see Figure S5), opening the route to prepare nanohybrids that are applicable for different resonance energy transfer experiments. Overall, the distances are well-suited for effective Förster-type resonance energy transfer (FRET) experiments. In contrast to earlier FRET experiments on another dye−QD system in blended films[15] or layer-by-layer films,[16] here we have a very narrow distribution of distances. This helps to evaluate energy transfer rates with much higher precision.

FRET System Using QD-535 as Donors and J-aggregates as Acceptors. First, we studied the excitonic energy transfer from QD-535 as donors to C8S3 J-aggregates as acceptors. For both components involved, the absorption and emission spectra are presented in Figure 3a. The photoluminescence maximum of QDs is located at 535 nm, which provides sufficient overlap with the J-band absorption of J-aggregates at 550−600 nm. The emission peak of the J-aggregates is centered at 600 nm and has negligible overlap with the QD-535 emission. To ensure efficient energy transfer, direct excitation of the acceptor has to be minimized. Although the absorbance of both species extends into the blue and UV region of the spectrum, a minimum excitation of J-aggregates relative to QD-535 excitation was identified at a wavelength of 380 nm by comparing the UV−vis spectra of the J-aggregate control and J-aggregate/QD-535 (see Figure 3b inset, where the logarithm of the spectra is plotted). In the J-aggregate/QD-535 nanohybrids, the photoluminescence intensity at 535 nm is significantly quenched to 8% of that from pure QD-535 solution (Figure 3b).

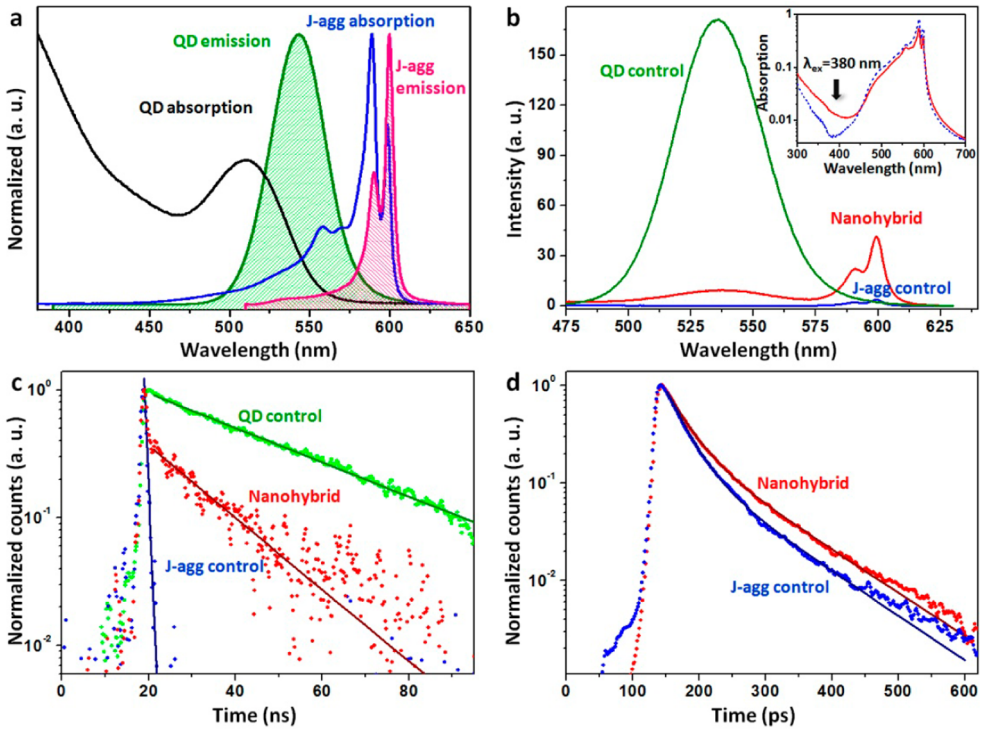

Figure 3. Optical spectra of J-aggregate/QD-535 nanohybrids to illustrate FRET from QD-535 to the J-aggregate. (a) Absorption and emission spectra of C8S3 J-aggregate nanotubes (λ_{ex} = 535 nm) and QD-535 (λ_{ex} = 380 nm), normalized to maximum value. (b) PL spectra of the J-aggregate/QD-535 nanohybrids, as well as QD-535 and J-aggregate controls (λ_{ex} = 380 nm), recorded at comparable respective concentrations and identical conditions. The inset shows the absorbance spectrum of the nanohybrids (red solid line) and the J-aggregate control (blue dashed line) in semi-logarithmic scale. (c) Time-resolved decay of PL emission at 535 ± 10 nm in J-aggregate/QD-535 nanohybrids, as well as QD-535 and J-aggregate controls, both curves normalized to maximum intensity. (d) Time-resolved decay of PL emission at 600 ± 3 nm in J-aggregate/QD-535 nanohybrids and J-aggregate control, normalized to maximum intensity.

Simultaneously, the photoluminescence (PL) of the J-aggregates at 600 nm is increased by a factor of more than 10.

The FRET was further confirmed by time-resolved emission spectroscopy. The time-resolved PL of J-aggregate/QD-535 nanohybrids was investigated using a streak camera with femtosecond pulsed laser excitation (for details, see the Supporting Information). A detection wavelength of 535 ± 10 nm was chosen to study the dynamics of the QD-535 emission (see Figure S4 for details). Figure 3c reveals the normalized PL decay curves of QD-535 in solution and QD-535 in J-aggregate/QD-535 nanohybrids. Without coupling to J-aggregates, QD-535 shows a single-exponential PL decay with a lifetime (τ_D) of 32.0 ± 0.4 ns. In the hybrid system, however, the PL decay of QD-535 does not follow a single-exponential decay, any more but exhibits two distinct decay modes: a very fast decay (below 500 ps) down to approximately 30% of the initial intensity and a slow decay which may be composed of several exponential decays, starting with a lifetime of 15.0 ± 0.4 ns (indicated as straight line) and extending to decay with the lifetime of the QD-535 control solution (32.0 ns). The slow decay was not fitted because of the high noise level. Hence, the normalized time-dependent intensity, $i_{DA}(t)$, can be described by a double-exponential decay given by $i_{DA}(t) = e^{-t/\tau_1} + ae^{-t/\tau_2}$ with τ_1 = 0.1 ns, τ_2 = 15 ns, and $a \cong 0.3$. The emission decay of a J-aggregate solution was also measured under the same conditions (Figure 3c). The J-aggregate, emission decay at this wavelength range is much faster, namely on the order of a few tens of picoseconds. Therefore, the PL of the acceptor (*i.e.*, the J-aggregates control) was recorded with better time resolution at an emission wavelength of 600 ± 3 nm, as shown in Figure 3d for both the J-aggregate control and the J-aggregate/QD-535 nanohybrids. The emission decay of the J-aggregate control follows a multiexponential decay, but in the time period below 400 ps (which includes 99% of emission intensity), a double-exponential decay fits very well. The only difference between the two samples is a slight increase of the decay time of the J-aggregate/QD-535 nanohybrids (τ_1 = 29 ± 0.2 ps, τ_2 = 98 ± 1 ps, A_1/A_2 = 2.59) compared to J-aggregates (τ_1 = 27 ± 0.3 ps, τ_2 = 83 ± 3 ps, A_1/A_2 = 3.4).

In order to interpret the data, we use Förster theory of resonant excitation energy transfer.[1,30,31] Therefore, we assume that the optical properties of the two constituents, the semiconducting QDs and the J-aggregates, are solely described by their transition dipoles, and dipole−dipole coupling is the primary mechanism for excitonic energy transfer. The total rate of energy

transfer $k^{(2)}_{D-A}$ is given by the sum over all rates from a single donor to all accessible acceptors:

$$k^{(2)}_{D-A} = \frac{1}{\tau_D}\sum_i \kappa_i^2(r_i, \Omega_i)\,\frac{R_F^6}{r_i^6} \quad (1)$$

Here, r_i denotes the center-to-center distances between donor and acceptors i, $\kappa^2(r_i, \Omega_i)$ is a factor taking into account the mutual orientation of the dipoles, and R_F is the Förster radius, calculated without any orientation factor, or taking $\kappa^2 = 1$. The Förster radius is determined from the spectral overlap of the QD-535 emission and the J-aggregates absorption to be $R_F = 4.7$ nm (see Supporting Information for details).

In order to simplify the calculations, we assume that the donor QDs are sitting on top of a planar layer of dye molecules; that is, we neglect the curvature of the cylindrical aggregate. This assumption is justified because the typical distance between a donor particle and the surface of the J-aggregate is in the range of 3 to 4 nm, less than the radius of the tube (6.5 nm). Notable energy transfer will be within a sphere of approximately $2R_F$ around the donor. Within this sphere, it is acceptable to neglect the curvature of the cylinder. Additionally, we neglect the double-layer structure of the tubular dye aggregates and consider only the outer layer of dyes. This is justified because the spectral overlap between donor emission and the absorption band of the outer layer (at about 590 nm)[26,32] is better than with the absorption band of the inner layer (at 600 nm). The J-aggregate bands at a shorter wavelength are less clearly understood; they probably belong to both walls and therefore are not considered to be important.[32] Additionally, the inner layer of the J-aggregate nanotube is at a larger distance to the donor, and the majority (about 60%) of dyes are located at the outer wall.

Under these assumptions, the energy transfer rate is described by the known formula for layered systems[23]

$$k^{(2)}_{D-A} = \left(\frac{1}{\tau_D}\right)\left(\frac{d_0}{d}\right)^4, \text{with } d_0^4 = \sigma\gamma R_0^6/\kappa^2 \quad (2)$$

and the total transfer efficiency is given by

$$E^{(2)} = \frac{d_0^4}{d_0^4 + d^4} \quad (3)$$

Here, σ denotes the mean density of dye molecules per area, and γ is a new factor, taking into account the mean mutual orientation of the dipoles. Assuming that all acceptors are oriented in parallel within a plane and that the donors are oriented randomly, one obtains $\gamma = \pi/4$.[19] The density σ is evaluated from the typical cross sectional area of one dye molecule to be about 1/0.6 nm^{-2}. Using the Förster radius and other constants as above, one obtains $d_0 = 10.9$ nm.

It is notable that this assumption is even true for the case of delocalized excitons. The extended excitons may be addressed by a center molecule, but every molecule within the aggregate may serve as such a center. Therefore, the "density" of excitons, which may be excited from a single donor, is identical to the density of molecules, independent of the size of the exciton.

The experimental value of the transfer efficiency is obtained from steady-state and time-resolved fluorescence by

$$E_{x,s} = 1 - \frac{I_{DA}}{I_D} \quad (4)$$

$$E_{x,t} = 1 - \frac{\int i_{DA}(t)\mathrm{d}t}{\int i_D(t)\mathrm{d}t} \quad (5)$$

respectively, where $I_{DA}(t)$ and $I_D(t)$ are the steady fluorescence intensity of the donor with or without acceptor, respectively, and $i_{DA}(t)$ and $i_D(t)$ are the corresponding dynamic fluorescence intensities.

From the donor quenching, as shown in Figure 3b, a steady-state transfer efficiency is evaluated to be $E_{x,s} = 0.92$. Using the double-exponential decay in Figure 3c, the dynamic transfer efficiency is calculated to be $E_{x,t} = 1 - (\tau_1 + a\tau_2/\tau_D) = 0.86$. Both values are quite close, showing that about 90% of the excitation energy of the donors is transferred to acceptors.

Applying these results to eq 3 allows the calculation of an expected mean distance between donor particles and J-aggregate, which comes out to be 5.9 nm. This distance is larger than the typical increase in the radius of the J-aggregates demonstrated in Figure 2c.

In a reverse calculation, we measure the typical distances between particles and the J-aggregate surface from the cryo-TEM images (Figure 2c,d) and evaluate the corresponding energy transfer efficiencies. In order to extract the mean center-to-center distance between the transition dipoles of the particles and the dyes of the outer layer of the J-aggregates, one has to take into account the size of the particles (2−3 nm in diameter) and the distance between the outer J-aggregate surface and position of the chromophores (*i.e.*, the conjugated π-electron system, which is typically 1 nm separated from the surface). If J-aggregates are densely covered by particles, as shown in Figure 2c, one obtains a typical distance of approximately 2.5 to 3.5 nm and the corresponding transfer efficiency is from 98 to 99.7%. If aggregates are loosely covered by particles, as shown for the thorn-like hybrid structures in Figure 3d, distances are on the order of a ten nanometers and one estimates efficiencies on the order of 50%.

An inhomogeneous distribution of the donor particles on the J-aggregates may explain the mismatch between the calculated transfer efficiency and the observed total efficiency. The particles located close to the J-aggregates as in Figure 2c do have energy

transfer efficiencies close to 100%, and their emission is totally quenched. The remaining emission of about 8% recorded in the spectrum of Figure 3b results from particles that are more loosely bound to the aggregates and at larger distances, as in Figure 2d. Thus, one expects that in a spatially resolved image, showing only one J-aggregate, one would see the remaining emission of donor QDs for the thorn-like J-aggregates while the others become dark.

This interpretation is also in accordance with the time-resolved data. The majority of QDs that are close to J-aggregates (probably about 70%, as concluded from the factor *a* of the double-exponential decay curve) cause the fast PL decay, due to the fast time constant of energy transfer. The latter is calculated from the transfer rate at distance d_0 to be less than 3 ps, far below the resolution limit of the streak camera used in Figure 2c. About 30% of particles are believed to be at larger distances with a PL decay time of about one-half of their native lifetime. They become apparent only when the intensity has significantly decreased by the first fast decay. This explains the kink in the lifetime measurement shown in Figure 3c.

FRET System Using J-Aggregate as Donor and QD-665 as Acceptor. The size-dependent excitation energy of the QDs (quantum confinement) allows the reversal of the energy transfer pathway. Here now, QDs with lower excitation energy (QD-665, $\lambda_{em} = 665$ nm) were used to study energy transfer from the J-aggregate to the QDs. Such a system is particularly suited for photoconversion because it utilizes the strong absorbance of the J-aggregates to funnel light energy into the inorganic particles. This can be considered as a prototype of an artificial light-harvesting system and was realized using similar methods as discussed above with larger QDs (QD-665, $\lambda_{em} = 665$ nm) with an emission red-shifted compared to that of J-aggregates. QD-665 serves here as an acceptor, while the J-aggregate serves as a donor. The morphology of the J-aggregates decorated with QD-665 appears similar to the J-aggregate/QD-535 (see Figure S5, Supporting Information). This is reasonable because the surface chemistry of QD-665 and QD-535 is identical (with the same surface capping ligands). Also, we do not expect significant differences in the binding of the QDs to the J-aggregates, which is mostly governed by electrostatic forces.

As shown in Figure 4a, the J-band emission of the J-aggregate at 600 nm overlaps with the absorption spectrum of QD-665 but not with the QD-665 emission. The spectral overlap is of similar magnitude as it was in the previous system (Figure 3a). However, it is impossible to analyze the energy transfer in a "symmetric" way as presented in the J-aggregate/QD-535 system. This is due to the asymmetry of our FRET systems: First, the concentration of particles is always much less than the concentration of dyes. In the case of J-aggregate/QD-535, the donors represent the minority group, while in the case of J-aggregate/QD-665, the acceptors are the minority group. Second, in the case of J-aggregate/QD-535 nanohybrids, the particles (donors) can be excited without exciting the dyes (acceptor). In the case of J-aggregate/QD-665 nanohybrids, the excitation of the J-aggregate (donor) is always accompanied by excitation of the particles (acceptors). Due to these asymmetries, in both cases, the signal of the minority partner has to be monitored to analyze the FRET. Therefore, to investigate the FRET from the J-aggregates to the QD-665, the emission of the donor QDs is used to evaluate the energy transfer efficiency.

The main evidence for FRET is the enhanced emission of the QD-665 particles when excited *via* the J-band absorption. In Figure 4b, the absorption spectra of the J-aggregate/QD-665 nanohybrid and a pure QD-665 solution are shown. The absorbance of the pure QD-665 solution was scaled to fit the corresponding absorbance of the nanohybrid spectrum. The absorbance of the hybrids at 589 nm is found to be approximately 20 times higher than the absorbance of the pure QDs. The maximum of the J-aggregate absorption was chosen to excite the nanohybrid photoluminescence as presented in Figure 4c. The PL emission of the nanohybrids at 665 nm is enhanced by a factor of approximately 10 compared to that of the QD-665 control solution. The shape of the emission spectrum remains unaltered.

More insight into the transfer mechanism is gained from photoluminescence excitation (PLE) measurements ($\lambda_{em} = 665$ nm). In Figure 4d, the excitation spectra of pure QD-665 solution and nanohybrids are presented, with the latter showing excitation spectrum similar to J-band absorption. At the wavelength of 589 nm, the intensity is increased by a factor of 10, consistent with the intensity enhancement of the emission shown in Figure 4c. However, the shape of the excitation spectrum is distorted compared to the absorption of the J-aggregates. It is very much broadened, and the narrow absorption peaks seem to be smeared out. Additionally, the maximum is now at 600 nm, which corresponds to the absorption band that is usually assigned to the inner wall of the double-layer structure of the tubular J-aggregate.[17] These spectral changes may be either due to static disorder of the aggregates in the vicinity of the acceptor particles, or due to dynamic distortion of the spectrum and the fast transfer time.

Irrespective of this spectral distortion, a more quantitative analysis of the PLE spectrum was used[22] in order to extract the energy transfer efficiency. Therefore, the effective absorption spectrum of the QD-665 was evaluated from the PLE spectrum of the J-aggregate/QD-665 nanohybrids. The effective absorption represents the spectral absorption that leads to emission of the QD-665 at 665 nm and is expressed

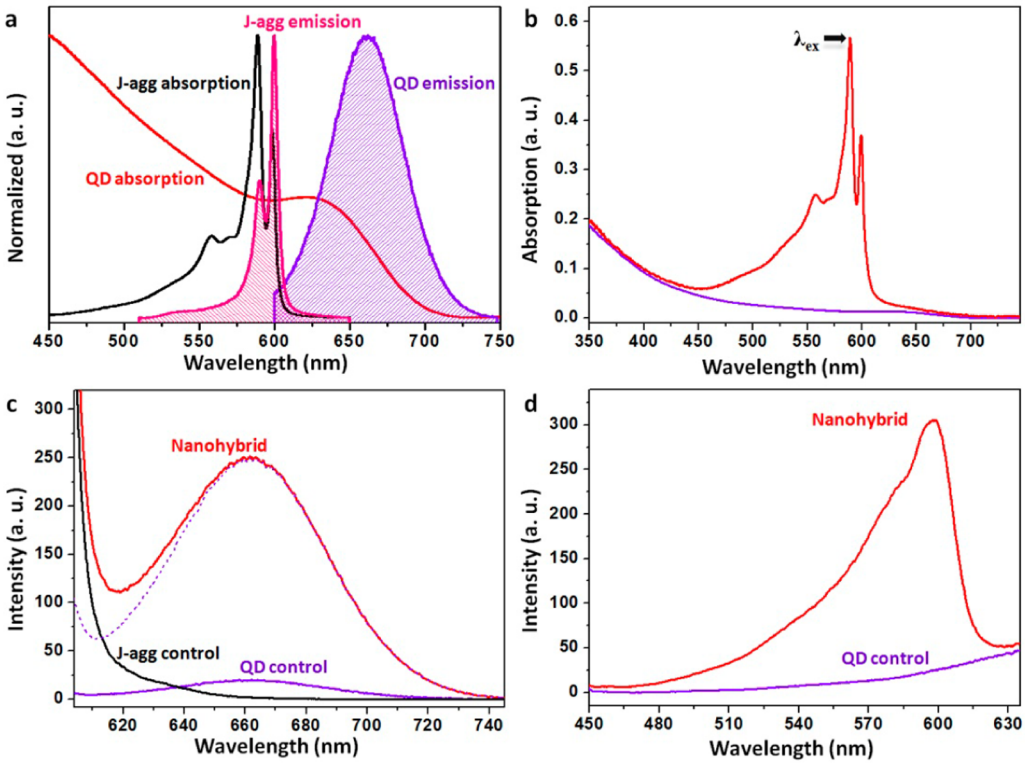

Figure 4. Optical characterizations of J-aggregate/QD-665 nanohybrids to explore the resonance energy transfer from the J-aggregate to QD-665. (a) Absorption and emission spectra of C8S3 J-aggregates (λ_{ex} = 500 nm) and QD-665 (λ_{ex} = 600 nm), normalized to maximum value. (b) Absorption spectra of J-aggregate/QD-665 nanohybrids (red) and QD-665 (purple). (c) PL spectra of the J-aggregate/QD-665 nanohybrids, as well as of QD-665 and C8S3 J-aggregate controls. The excitation wavelength was set to λ_{ex} = 589 nm, which is the peak of J-band absorption. By subtracting the contribution of the J-aggregate control, the sole emission spectrum of QD-665 in the hybrid system was obtained (purple dashed line). (d) PL excitation (PLE) spectra of J-aggregate/QD-665 nanohybrids and QD-665, recorded at the emission of 665 nm.

as ($A^J \times E + A^{QD}$), where A^J and A^{QD} are the absorptions of J-aggregates and QD-665, respectively, and E is the energy transfer efficiency. In order to convert the measured intensities into absorbance, the spectrum is compared to the PLE spectrum of another substance with known absorption spectrum. In this case, Nile Blue was used (Figure S6, Supporting Information). From the ratio between the effective absorption and the true absorption of pure J-aggregate solution, corrected by the absorbance of pure QD-665, the energy transfer efficiency is obtained to be approximately 20%. This is much less than the 92% efficiency of the reverse process, where the QDs serve as donors. At this stage, one may only speculate about the reason for this striking asymmetry of the energy transfer efficiency. One reason could be the inhomogeneities of the sample, which might cause spectral contributions of aggregates and particles that do not participate in energy transfer but show up in the respective spectra. Another reason may be the fact that in this situation energy transfer preferentially occurs from the inner wall of the double layer tubular J-aggregate. Even when excited in the outer wall, the excitation energy is transferred very fast (less than a picosecond)[33,34] to the inner wall. The energy transfer to the QD-665 then starts from the inner cylinder, which means the distance has increased and the efficiency is reduced. A third reason may be related to the mobility and extension of the Frenkel exciton within the J-aggregate. The extended exciton is known to diffuse (migrate) within the aggregate during its lifetime.[35] Due to this diffusion process, the exciton may be considered as an entity that is smeared out by the typical diffusion length during its lifetime. The mean distance for energy transfer thus is enlarged by this smearing effect. However, to our knowledge, there is yet no concise theoretical description of this dynamical effect.

CONCLUSIONS

To conclude, quasi-1D colloidal nanohybrid structures comprising cyanine dye J-aggregates decorated with semiconducting QDs were designed through an electrostatic self-assembly method. Negatively charged QDs with different emission wavelengths (*i.e.*, 535 and 665 nm) were successfully assembled on the supramolecular J-aggregate nanotubes using a polycation layer of PDADMAC as molecular glue. This method leaves the J-aggregates structurally unaffected and allows combination with QDs of various size and optical properties. The structural organization of these nanohybrids is unprecedented, and the concept of fabrication can easily be extended to combine the J-aggregates with

other inorganic materials given that they have a chemical coating that provides negative surface charges.

Strong energy transfer from the QDs to the J-aggregate and from the J-aggregate to the QDs could be demonstrated, whereas the direction of energy transfer is switched by the QDs size and hence optical properties. A remarkable asymmetry of the transfer efficiency was observed, as it was 92% for the case of transfer from the QDs, while it achieved 20% in the case of transfer to the QDs. Although at this stage we cannot exclude trivial reasons for this effect (such as structural inhomogeneity not seen by the local inspection of cryo-TEM), we consider it as an interesting effect that should be investigated further, probably on isolated single aggregates using local spectroscopy methods. The very strong coupling between the inorganic semiconductors and the tubular J-aggregates is promising for the search for coherent coupling effects, which are expected for such systems within the strong coupling regime.[5] Due to the well-defined structural composition, a detailed insight into the photophysical properties of such organic–inorganic hybrid systems can be obtained, which will be helpful for the understanding of hybrid inorganic–organic systems in general.

EXPERIMENTAL SECTION

Preparation of Tubular J-Aggregates. J-aggregate nanotubes were prepared in water/methanol solution following the so-called "alcoholic route".[19] Stock solution of C8S3 (2.92 mM) was prepared by directly dissolving C8S3 powder (FEW Chemicals, Germany) in methanol (≥99.9% GC, Sigma-Aldrich). Then 130 μL of the C8S3 stock solution was added to 500 μL of ultrapure H_2O followed by thorough vortex spinning to ensure complete mixing. An immediate color change of the solution (from orange to deep pink) was observed, indicating the formation of tubular J-aggregates. The solution was stored in the dark for 24 h before adding an additional 500 μL of ultrapure H_2O to stabilize the aggregation process, resulting in a final concentration of 0.336 mM. Fresh J-aggregate solutions were stored in the dark and used within 3 days after preparation.

Preparation of QD Solution. QD-535 (emission = 530 ± 5 nm) and QD-665 (emission = 670 ± 5 nm) were bought from PlasmaChem GmbH (Germany) and used as received. The QD solutions were prepared by dispersing MPA-capped CdTe QD powders in ultrapure H_2O with desired concentrations. The samples were stored in a refrigerator and dispersed with an ultrasonic instrument before use (4 °C).

Preparation of J-Aggregate/QD Nanohybrids *via* Electrostatic Self-Assembly. In a typical process, 8 μL of PDADMAC (average M_w 100 000–200 000, Sigma-Aldrich) solution with 1 mM monomer concentration was added to a 100 μL of C8S3 J-aggregate solution. The solution was kept in the dark for 3 h before adding 20 μL of MPA-capped CdTe QD solution (0.5 mg/mL). The final solution was stored for at least another 3 h to reach equilibrium before characterization. The J-aggregate control samples are made by addition of 8 μL of PDADMAC solution (1 mM monomer concentration) and 20 μL of ultrapure H_2O to 100 μL of C8S3 J-aggregate solution. The QD control samples are made by addition of 20 μL of MPA-capped CdTe QDs solution (0.5 mg/mL) to 108 μL of ultrapure H_2O.

Cryogenic Transmission Electron Microscopy. Droplets of the solution (5 μL) were applied to carbon film (1 μm hole diameter) covered 200 mesh grids (R1/4 batch of Quantifoil Micro Tools GmbH, Jena, Germany), which had been hydrophilized before use by plasma processing. Supernatant fluid was removed by Vitrobot Mark IV (FEI, linux operating system) until an ultrathin layer of the sample solution was obtained that spanned the holes of the carbon film. The samples were immediately vitrified by propelling the grids into liquid ethane at its freezing point (90 K) with a plunging device. Frozen samples were transferred into the TEM (JEOL JEM2100, Germany) using a JEOL cryoholder and transfer station. Microscopy was carried out at a 94 K sample temperature using the microscope's low-dose protocol at a calibrated primary magnification of 20 000× and an accelerating voltage of 200 kV (LaB6-illumination). The defocus was chosen to be 1.2 mm to create sufficient phase contrast for imaging. Image analysis was performed with ImageJ software.

Absorption Spectroscopy. Absorption spectra of the solution were taken with a double-beam UV–vis spectrometer (Shimadzu UV-2101PC, revision 2.2) in a 0.2, 1.0, or 10.0 mm quartz cell (Hellma GmbH, Germany).

Fluorescence Spectroscopy. Fluorescence spectra were taken on a fluorescence spectrometer (JASCO FP 6500) in quartz cells (Hellma GmbH, Germany) with the path length of 0.2, 1.0, or 10.0 mm. The fluorometer came with a built-in light source (Xe lamp UXL-159, 150 W) and two grating monochromators with variable slit width and detector.

Time-Resolved Fluorescence Spectroscopy. Transient photoluminescence spectroscopy was carried out using a femtosecond laser (Tsunami, Spectra Physics) and a streak camera (CS5680, Hamamatsu) connected to a 30 cm spectrograph. The laser was frequency-doubled for excitation at 380 nm. To avoid accumulation effects in the measurement of the QDs, a pulse picker was used to reduce the pulse repetition rate to 370 kHz. The full repetition rate of 80 MHz was applied for the measurements of the J-aggregates with the streak camera in Synchroscan mode to obtain the required temporal resolution on the order of 10 ps. In all cases, the pump fluence was kept below 5 W/cm^2 in order to avoid the excitation of multiple excitons in the sample. In addition, the sample was continuously moved during data acquisition to prevent photodamage to the J-aggregate. Special care was taken to protect the samples from any room light during handling and during the measurement.

The photoluminescence decay curves were extracted from the streak images by integrating the intensity over a wavelength interval of 525 to 545 nm for the QDs and of 597 to 603 nm for the J-aggregates. For the QDs, good least-squares fits could be obtained using a single-exponential function. Fitting of the J-aggregate transients required an exponential function with two decay constants.

Conflict of Interest: The authors declare no competing financial interest.

Acknowledgment. We thank the Deutsche Forschungsgemeinschaft (collaborative research center SFB 951) for financial support. We thank Dr. Omar Al-Khatib and Evi Poblenz, both at Humboldt-Universität, for fruitful discussions and assistance, respectively. F. P. gratefully acknowledges the Joint Lab for Structural Research Berlin within IRIS Adlershof for funding.

Supporting Information Available: Additional cryo-TEM images, optical spectra for pure J-aggregates together with fluorescence excitation spectra, determination of the quantum efficiencies of the QDs and the J-aggregates. This material is available free of charge *via* the Internet at http://pubs.acs.org.

REFERENCES AND NOTES

1. Medintz, I. L.; Mattoussi, H. Quantum Dot-Based Resonance Energy Transfer and Its Growing Application in Biology. *Phys. Chem. Chem. Phys.* **2009**, *11*, 17–45.
2. Savateeva, D.; Melnikau, D.; Lesnyak, V.; Gaponik, N.; Rakovich, Y. P. Hybrid Organic/Inorganic Semiconductor Nanostructures with Highly Efficient Energy Transfer. *J. Mater. Chem.* **2012**, *22*, 10816–10820.

3. Heliotis, G.; Itskos, G.; Murray, R.; Dawson, M. D.; Watson, I. M.; Bradley, D. D. C. Hybrid Inorganic/Organic Semiconductor Heterostructures with Efficient Non-radiative Energy Transfer. *Adv. Mater.* **2006**, *18*, 334–338.
4. Blumstengel, S.; Sadofev, S.; Xu, C.; Puls, J.; Henneberger, F. Converting Wannier into Frenkel Excitons in an Inorganic/Organic Hybrid Semiconductor Nanostructure. *Phys. Rev. Lett.* **2006**, *97*, 237401.
5. Agranovich, V. M.; Basko, D. M.; La Rocca, G. C.; Bassani, F. Excitons and Optical Nonlinearities in Hybrid Organic–Inorganic Nanostructures. *J. Phys.: Condens. Matter* **1998**, *10*, 9369–9400.
6. Wuerthner, F.; Kaiser, T. E.; Saha-Moeller, C. R. J-Aggregates: From Serendipitous Discovery to Supramolecular Engineering of Functional Dye Materials. *Angew. Chem., Int. Ed.* **2011**, *50*, 3376–3410.
7. Kobayashi, T. *J-Aggregates*; World Scientific: Singapore, 1996.
8. Sengupta, S.; Wuerthner, F. Chlorophyll J-Aggregates: From Bioinspired Dye Stacks to Nanotubes, Liquid Crystals, and Biosupramolecular Electronics. *Acc. Chem. Res.* **2013**, *46*, 2498–2512.
9. Tian, Y.; Stepanenko, V.; Kaiser, T. E.; Wuerthner, F.; Scheblykin, I. G. Reorganization of Perylene Bisimide J-Aggregates: From Delocalized Collective to Localized Individual Excitations. *Nanoscale* **2012**, *4*, 218–223.
10. Scheblykin, I. G.; Varnavsky, O. P.; Bataiev, M. M.; Sliusarenko, O.; Van der Auweraer, M.; Vitukhnovsky, A. G. Non-coherent Exciton Migration in J-Aggregates of the Dye THIATS: Exciton–Exciton Annihilation and Fluorescence Depolarization. *Chem. Phys. Lett.* **1998**, *298*, 341–350.
11. Eisfeld, A.; Briggs, J. S. The J- and H-Bands of Organic Dye Aggregates. *Chem. Phys.* **2006**, *324*, 376–384.
12. Alivisatos, A. P. Semiconductor Clusters, Nanocrystals, and Quantum Dots. *Science* **1996**, *271*, 933–937.
13. Murray, C. B.; Kagan, C. R.; Bawendi, M. G. Synthesis and Characterization of Monodisperse Nanocrystals and Close-Packed Nanocrystal Assemblies. *Annu. Rev. Mater. Sci.* **2000**, *30*, 545–610.
14. Medintz, I. L.; Uyeda, H. T.; Goldman, E. R.; Mattoussi, H. Quantum Dot Bioconjugates for Imaging, Labelling and Sensing. *Nat. Mater.* **2005**, *4*, 435–446.
15. Schlamp, M. C.; Peng, X. G.; Alivisatos, A. P. Improved Efficiencies in Light Emitting Diodes Made with CdSe(CdS) Core/Shell Type Nanocrystals and a Semiconducting Polymer. *J. Appl. Phys.* **1997**, *82*, 5837–5842.
16. Dabbousi, B. O.; Bawendi, M. G.; Onitsuka, O.; Rubner, M. F. Electroluminescence from CdSe Quantum-Dot Polymer Composites. *Appl. Phys. Lett.* **1995**, *66*, 1316–1318.
17. Osedach, T. P.; Iacchetti, A.; Lunt, R. R.; Andrew, T. L.; Brown, P. R.; Akselrod, G. M.; Bulovic, V. Near-Infrared Photodetector Consisting of J-Aggregating Cyanine Dye and Metal Oxide Thin Films. *Appl. Phys. Lett.* **2012**, *101*, 113303.
18. Sandquist, C.; McHale, J. L. Improved Efficiency of Betanin-Based Dye-Sensitized Solar Cells. *J. Photochem. Photobiol., A* **2011**, *221*, 90–97.
19. Stull, J. A.; Britt, R. D.; McHale, J. L.; Knorr, F. J.; Lymar, S. V.; Hurst, J. K. Anomalous Reactivity of Ceric Nitrate in Ruthenium "Blue Dimer"-Catalyzed Water Oxidation. *J. Am. Chem. Soc.* **2012**, *134*, 19973–19976.
20. McHale, J. L. Hierarchal Light-Harvesting Aggregates and Their Potential for Solar Energy Applications. *J. Phys. Chem. Lett.* **2012**, *3*, 587–597.
21. Walker, B. J.; Bulovic, V.; Bawendi, M. G. Quantum Dot/J-Aggregate Blended Films for Light Harvesting and Energy Transfer. *Nano Lett.* **2010**, *10*, 3995–3999.
22. Zhang, Q.; Atay, T.; Tischler, J. R.; Bradley, M. S.; Bulovic, V.; Nurmikko, A. V. Highly Efficient Resonant Coupling of Optical Excitations in Hybrid Organic/Inorganic Semiconductor Nanostructures. *Nat. Nanotechnol.* **2007**, *2*, 555–559.
23. Walker, B. J.; Dorn, A.; Bulovic, V.; Bawendi, M. G. Color-Selective Photocurrent Enhancement in Coupled J-Aggregate/Nanowires Formed in Solution. *Nano Lett.* **2011**, *11*, 2655–2659.
24. von Berlepsch, H.; Böttcher, C.; Ouart, A.; Burger, C.; Dähne, S.; Kirstein, S. Supramolecular Structures of J-Aggregates of Carbocyanine Dyes in Solution. *J. Phys. Chem. B* **2000**, *104*, 5255–5262.
25. von Berlepsch, H.; Kirstein, S.; Hania, R.; Pugzlys, A.; Böttcher, C. Modification of the Nanoscale Structure of the J-Aggregate of a Sulfonate-Substituted Amphiphilic Carbocyanine Dye through Incorporation of Surface-Active Additives. *J. Phys. Chem. B* **2007**, *111*, 1701–1711.
26. Eisele, D. M.; Knoester, J.; Kirstein, S.; Rabe, J. P.; Vanden Bout, D. A. Uniform Exciton Fluorescence from Individual Molecular Nanotubes Immobilized on Solid Substrates. *Nat. Nanotechnol.* **2009**, *4*, 658–663.
27. Qiao, Y.; Polzer, F.; Kirmse, H.; Steeg, E.; Kirstein, S.; Rabe, J. P. In Situ Synthesis of Semiconductor Nanocrystals at the Surface of Tubular J-Aggregates. *J. Mater. Chem. C* **2014**, *2*, 9141–9148.
28. Prokhorenko, V. I.; Steensgaard, D. B.; Holzwarth, A. R. Exciton Theory for Supramolecular Chlorosomal Aggregates: 1. Aggregate Size Dependence of the Linear Spectra. *Biophys. J.* **2003**, *85*, 3173–3186.
29. Yuan, J.; Müller, A. H. E. One-Dimensional Organic–Inorganic Hybrid Nanomaterials. *Polymer* **2010**, *51*, 4015–4036.
30. Kuhn, H. Classical Aspects of Energy Transfer in Molecular Systems. *J. Chem. Phys.* **1970**, *53*, 101–108.
31. Richter, B.; Kirstein, S. Excitation Energy Transfer between Molecular Thin Layers of Poly(phenylene vinylene) and Dye Labeled Poly(allylamine) in Layer-by-Layer Self-Assembled Films. *J. Chem. Phys.* **1999**, *111*, 5191–5200.
32. Clark, K. A.; Cone, C. W.; Vanden Bout, D. A. Quantifying the Polarization of Exciton Transitions in Double-Walled Nanotubular J-Aggregates. *J. Phys. Chem. C* **2013**, *117*, 26473–26481.
33. Yuen-Zhou, J.; Arias, D. H.; Eisele, D. M.; Steiner, C. P.; Krich, J. J.; Bawendi, M. G.; Nelson, K. A.; Aspuru-Guzik, A. Coherent Exciton Dynamics in Supramolecular Light-Harvesting Nanotubes Revealed by Ultrafast Quantum Process Tomography. *ACS Nano* **2014**, *8*, 5527–5534.
34. Milota, F.; Prokhorenko, V. I.; Mancal, T.; von Berlepsch, H.; Bixner, O.; Kauffmann, H. F.; Hauer, J. Vibronic and Vibrational Coherences in Two-Dimensional Electronic Spectra of Supramolecular J-Aggregates. *J. Phys. Chem. A* **2013**, *117*, 6007–6014.
35. Clark, K. A.; Krueger, E. L.; Vanden Bout, D. A. Direct Measurement of Energy Migration in Supramolecular Carbocyanine Dye Nanotubes. *J. Phys. Chem. Lett.* **2014**, *5*, 2274–2282.